ACS APPLIED MATERIALS & INTERFACES

www.acsami.org

Research Article

Stand-Alone CdS Nanocrystals for Photocatalytic CO_2 Reduction with High Efficiency and Selectivity

You-Xiang Feng,[§] Hong-Juan Wang,[§] Jia-Wei Wang, Wen Zhang,* Min Zhang,* and Tong-Bu Lu*

Cite This: *ACS Appl. Mater. Interfaces* 2021, 13, 26573−26580

Read Online

ACCESS | Metrics & More | Article Recommendations | Supporting Information

ABSTRACT: The development of a cost-effective photocatalyst is highly anticipated to achieve efficient photocatalytic CO_2 reduction with superior selectivity, which is still facing the lack of valid settlements. Herein, 4-mercaptopyridine (PD) as the building block of a capping ligand is tightly decorated on the surface of CdS nanocrystals (CdS-PD) using a facile ligand-exchange strategy, to exploit a cost-effective photocatalyst for photocatalytic CO_2 reduction without any cocatalysts. The conjugated structure of PD can facilitate the delocalization of photogenerated electrons in CdS nanocrystals, bringing forth an improved charge separation efficiency. More importantly, N-protonated PD can enable the easy formation of a six-membered ring intermediate with CO_2 assisted by water, which can serve as the efficient active site to achieve photocatalytic CO_2 reduction. In the absence of a cocatalyst, stand-alone CdS-PD nanocrystals exhibit an excellent CO yield of 20.35 mmol g^{-1} h^{-1} concomitant with a high selectivity of 95.3% for the CO_2-to-CO conversion under visible light, which are remarkably superior than those of CdS nanocrystals possessing traditional alkyl-chain and other conjugated capping ligands.

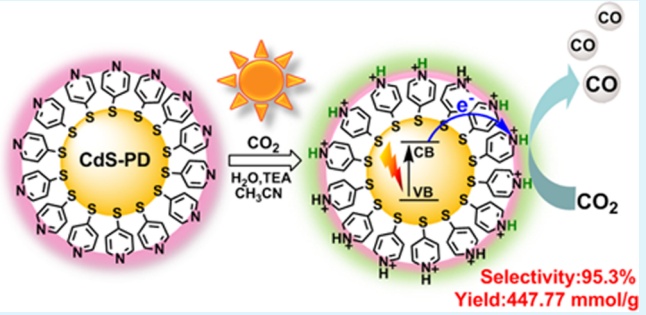

KEYWORDS: *charge transfer, CdS nanocrystals, CO_2 reduction, photocatalysis, pyridinium*

1. INTRODUCTION

The photocatalytic reduction of CO_2 to value-added products is of growing interest, which provides a promising pathway to develop sustainable energy and mitigate the greenhouse effect simultaneously.[1−4] Nevertheless, in comparison with hydrogen evolution,[5−10] the development of photocatalytic CO_2 reduction is still lagging behind because the CO_2 reduction reaction is far more complicated due to the chemical inertness of CO_2 itself and the diversity of products.[11−14] Therefore, exploiting a cost-effective photocatalyst for photocatalytic CO_2 reduction with high efficiency and selectivity is highly anticipated, which has attracted tremendous attention during the past decade.[15−21] In this regard, semiconductor nanocrystals (NCs) have been demonstrated to be one of the promising materials in artificial photosynthetic systems[22−27] due to their distinct photochemical and photophysical properties,[28−30] including excellent light harvesting,[31] tunable band alignment,[32,33] multiple exciton generation,[34] and rich surface binding sites.[35,36]

However, semiconductor NCs generally exhibit low activity for CO_2 reduction in their pristine forms, owing to the inferior charge separation. Therefore, they are usually used as a light absorber to cooperate with cocatalysts, such as metal complexes or other inorganic heterogeneous catalysts,[37−45] to achieve the improvement of photocatalytic performance. It is worth noting that the capping ligands are indispensable for maintaining the stability of semiconductor NCs, which will inevitably restrict the charge transfer between semiconductor NCs and cocatalysts.[46,47] Many strategies have been successfully developed to enhance the electronic communication from semiconductor NCs to a cocatalyst, by functionalizing the capping ligands to strongly bind the semiconductor NCs and the cocatalyst together through a covalent connection[48] or an electrostatic interaction,[49,50] greatly enhancing the photocatalytic activity and selectivity. Nevertheless, these strategies also lead to the complication and uncontrollability of a photocatalytic system, and the development of a simple and efficient semiconductor NC photocatalyst for CO_2 reduction still calls for valid settlements.

The exploitation of appropriate conjugated organic building blocks as capping ligands, extracting photogenerated electrons from semiconductor NCs and serving as the catalytic active center simultaneously, could be a feasible strategy for the construction of a cost-effective photocatalyst with high performance, which has attracted no attention yet. Herein, 4-

Received: February 24, 2021
Accepted: May 17, 2021
Published: May 26, 2021

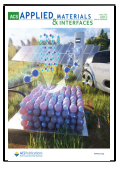

https://doi.org/10.1021/acsami.1c03606
ACS Appl. Mater. Interfaces 2021, 13, 26573−26580

Scheme 1. Schematic Diagrams of CdS NCs with Different Capping Ligands and the Photocatalytic Reduction Process of CdS-PD NCs for the Conversion of CO_2 to CO

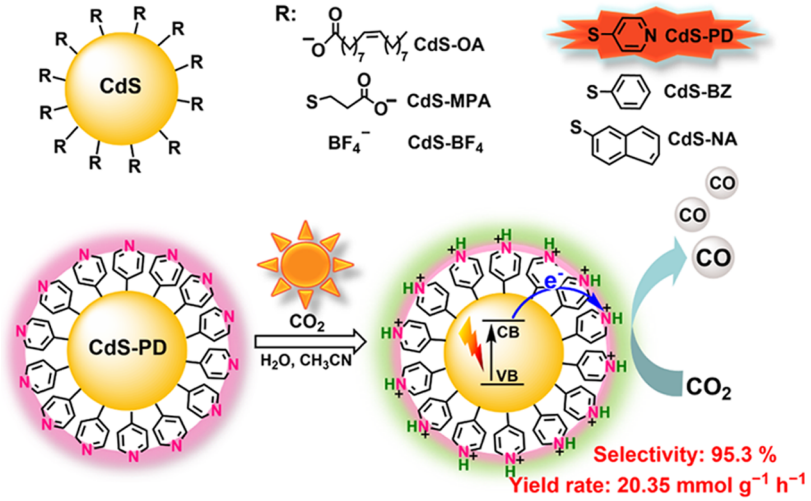

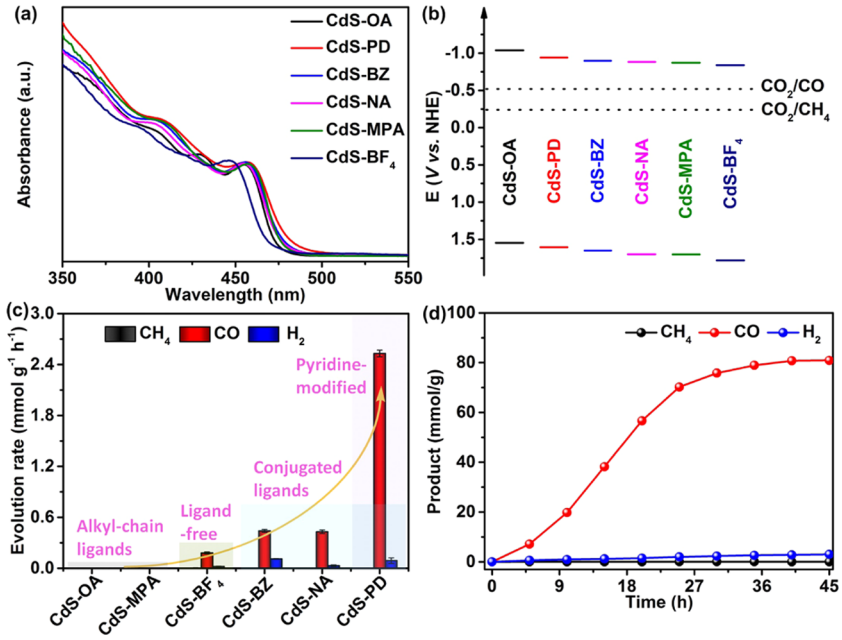

Figure 1. (a) UV−vis absorption spectra, (b) band structures, and (c) the CO yields of CdS-R NCs (R = OA, PD, BZ, NA, MPA, and BF_4). (d) Tracing of CO evolution over CdS-PD NCs. Reaction conditions: CdS NCs (1 μM), triethylamine (0.3 M), 5 mL of CH_3CN, 25 °C, a 300 W Xe lamp ($\lambda \geq 420$ nm, 250 mW cm^{-2}), 22 h.

mercaptopyridine was selected as the blocking ligand and decorated on the surface of CdS NCs (CdS-CD) for the following two reasons. First, different from the insulating alkyl-chain ligand, the conjugated structure of PD can facilitate the delocalization of photogenerated electrons in CdS nanocrystals, bringing forth the improved charge separation efficiency. Second, pyridinium has been successfully employed as the metal-free active site for the electroreduction and photoreduction of CO_2.[51−53] Unfortunately, inferior activity and stability were observed for the pyridinium-based catalyst system, owing to the sluggish electron-transfer kinetics between the chromophore and pyridinium and the degradation of the photosensitizer.[53] The connection of PD on the surface of CdS nanocrystals can increase the active sites for CO_2 reduction and facilitate the electron communications between the photosensitizers and active sites. Herein, the decoration of 4-mercaptopyridine on the surface of CdS NCs (coded as CdS-PD) was conducted through the coordination of Cd and S atoms, to exploit a new and highly efficient photocatalyst for CO_2 reduction. The unique property of PD on the photocatalytic performance has been examined by comparing it with CdS NC characteristics of alkyl-chain or other conjugated capping ligands (Scheme 1) by conducting a joint structural, photophysical, electrochemical, and theoretical study.

2. EXPERIMENTAL SECTION

2.1. Preparation of CdS NCs. The oleic acid-capped CdS NCs (CdS-OA),[54] thiohydracrylic acid-capped CdS NCs (CdS-MPA),[33] and ligand stripping CdS-BF_4 NCs[54] were prepared according to the reported procedure.

Preparation of CdS-R NCs (R = PD, BZ, NA): First, 4-mercaptopyridine (3 mmol) was dissolved in methanol (10 mL),

https://doi.org/10.1021/acsami.1c03606
ACS Appl. Mater. Interfaces 2021, 13, 26573−26580

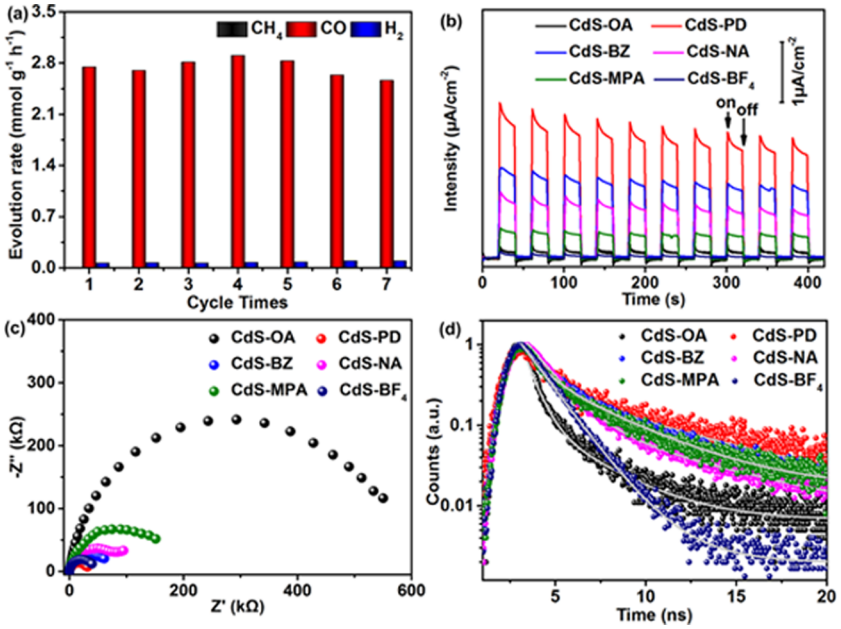

Figure 2. (a) Cycling experiments using CdS-PD NCs. (b) $I-t$ curves of CdS-R (R = OA, PD, BZ, NA, MPA, and BF_4) NCs at 0 V vs Ag/AgCl under light illumination. (c) Electrochemical impedance spectroscopy (EIS) Nyquist plots of CdS-R NCs under light illumination. (d) Photoluminescence (PL) decay curves of CdS-R NCs.

and the pH was adjusted to 10.5 with tetramethylammonium hydroxide (TMAOH). CdS-OA NCs (0.1 μmol) were added to this mixture and stirred in the dark for 48 h. After that, CdS-PD NCs were precipitated with excess acetone and centrifuged for separation (7000 rpm, 3 min). The obtained CdS-PD NCs were washed with acetone before being dispersed to dimethyl sulfoxide (DMSO). The same method was used to prepare CdS-BZ NCs and CdS-NA NCs, except for replacing 4-mercaptopyridine with mercaptobenzene and 2-mercaptonaphthalene, respectively.

2.2. Photocatalytic Experiments. The photocatalytic CO_2 reduction experiments were conducted in a 10 mL sealed quartz bottle with CdS-R (R = PD, BZ, NA, OA, MPA, and BF_4) NCs (1 μM) as catalysts, triethylamine (TEA) (0.3 M) as the electron sacrificial reagent, and CH_3CN (5 mL) as the solvent. Then, the reaction system was saturated with high-purity CO_2 and irradiated using a 300 W Xe lamp with a 420 nm cutoff filter at 25 °C; the light intensity was maintained at 250 mW cm^{-2}. The products (CO, CH_4, and H_2) in the gas phase were detected by gas chromatography.

3. RESULTS AND DISCUSSION

3.1. Structures and Optical Properties of CdS NCs. The ^{1}H nuclear magnetic resonance (NMR) measurement of CdS-PD NCs (Figure S1) shows that the pyridine groups have successfully replaced the oleic acid ligands on the CdS-OA precursor. The transmission electron microscopy (TEM) and dynamic light scattering (DLS) measurements (Figures S2 and S3) show that all of these CdS NCs display a similar average diameter, being approximately 5 nm, except for ligand-free CdS-BF_4 NCs, which have a smaller diameter (~4.0 nm). The size decrease of CdS-BF_4 NCs was mainly attributed to the etching of BF_4^- anions, which have strong binding interactions with Cd sites during the ligand stripping process.[55] The powder X-ray diffraction (XRD) results of all these CdS NCs with different surface ligands are identical, consistent with the crystal phase of cubic CdS (PDF no. 80-0019; Figure S4).

Ultraviolet−visible (UV−vis) absorption spectra and the Mott−Schottky plots were obtained to investigate the optical properties and the energy band structures of CdS NCs modified with different capping ligands. As shown in Figure 1a, the characteristic absorption peaks of CdS NCs with capping ligands are found at around 460 nm, while the absorption of ligand-free CdS-BF_4 NCs shows a blue shift of 10 nm, which are consistent with their size changes (Figures S2 and S3). After conversion to a plot of $(\alpha h\upsilon)^2$ vs photon energy, the direct band gaps of these CdS NCs were obtained and are shown in Figure S5. Additionally, as depicted in Figures S6 and1b, the flat band potentials of CdS NCs with different surface ligands were between −0.84 and −1.04 V vs normal hydrogen electrode (NHE) derived from the Motty−Schottky plots. The above results indicate that the conduction band values of these samples are all above −0.53 V vs NHE (CO_2-to-CO) and −0.25 V vs NHE (CO_2-to-CH_4), which are thermodynamically feasible for the photocatalytic conversion of CO_2 to CO or CH_4 (Figure 1b), suggesting that all of the prepared CdS NCs may serve as potential photocatalysts for CO_2 reduction.

3.2. Photocatalytic Conversion of CO_2 to CO. With the understanding of fundamental photophysical properties, the above six CdS-R (R = PD, BZ, NA, OA, MPA, and BF_4) NCs were investigated for CO_2 reduction under visible light irradiation ($\lambda \geq 420$ nm). The CO_2 reduction experiments were conducted in a 10 mL CO_2-purged quartz bottle containing CdS-R NCs, triethylamine (TEA), and CH_3CN. The main product was detected as CO concomitant with trace amounts of H_2 and CH_4 evolution. Among them, the entry with CdS-PD NCs exhibits the best photocatalytic performance for CO_2 reduction (Figure 1c), achieving a high CO yield of 2.56 mmol g^{-1} h^{-1} along with small amounts of CH_4 (0.4 μmol g^{-1} h^{-1}) and H_2 (0.1 mmol g^{-1} h^{-1}). For CdS-PD NCs, the selectivity and the apparent quantum yield (AQY) for CO_2 reduction to CO impressively approach 96.0 and 1.77%, respectively. In sharp contrast, much fewer amounts of CO were generated in the parallel photocatalytic experiments with pristine CdS-OA NCs (1 μmol g^{-1} h^{-1}) and CdS-MPA NCs (3 μmol g^{-1} h^{-1}) (Figure 1c), indicating that the alkyl-chain capping ligands disfavor the CO_2 reduction, possibly due to

https://doi.org/10.1021/acsami.1c03606
ACS Appl. Mater. Interfaces 2021, 13, 26573−26580

Table 1. Control and Amplified Experiments for CO_2 Reduction

entry	catalyst	n/H_2 (mmol g^{-1} h^{-1})	n/CO (mmol g^{-1} h^{-1})	n/CH_4 (mmol g^{-1} h^{-1})	selectivity to CO
1[a]	CdS-PD	0.94	20.35	0.06	95.3%
2	CdS-PD	0.10	2.56	0.0005	96.0%
3[b]	CdS-PD	0	0	0	0
4[c]		0	0	0	0
5[d]	CdS-PD	0	0.002	0.003	35.0%
6[e]	CdS-PD	0.61	0	0	0

[a]Entry 1: CdS-PD NCs (1 μM), triethylamine (0.3 M), 30 mL of CH_3CN with a 150 mL quartz bottle, 22 h, a 300 W Xe lamp ($\lambda \geq 420$ nm). [b]Entry 3: no light. [c]Entry 4: no CdS-PD NCs. [d]Entry 5: no TEA. [e]Entry 6: 100% Ar. Reaction conditions: CdS-PD NCs (1 μM), triethylamine (0.3 M), 5 mL of CH_3CN, 22 h, a 300 W Xe lamp ($\lambda \geq 420$ nm).

their insulating features that impede the electron-transfer processes. Notably, the photocatalysis in the same duration with the surface-ligand-free CdS-BF_4 NCs afforded a considerable CO yield of 0.19 mmol g^{-1} h^{-1} (Figure 1c), which can be ascribed to the exposed surface of CdS NCs that can mediate charge-carrier transfer. As shown in Figure 1c, the CdS-BZ NC and CdS-NA NC systems show significantly higher photocatalytic efficiency and selectivity for CO_2 reduction than CdS-OA NCs and CdS-MPA NC systems. These differences indicate that the aromatic ligands can accelerate the photocatalytic reaction. Importantly, despite all of the facilitative effects of ligand conjugation, the CO yields of CdS-PD NCs are about 5.6 and 6 times higher than those of the CdS-BZ NCs and CdS-NA NC systems (Figure 1c), respectively. Besides, when the total surface ligand content of pyridine and phenyl is fixed, the increasing of phenyl ligand will gradually reduce the catalytic activity of CdS NCs (Figure S7), demonstrating that the pyridine group is critical in promoting the CO_2 reduction rate of CdS NCs.

It is worth noting that the tracing diagram of the photocatalytic conversion of CO_2 to CO (Figure 1d) for CdS-PD shows that the CO evolution ceased after 45 h of irradiation. To explore the origin of deactivation, we carried out recycling experiments (Figure 2a) and found that the CdS-PD NCs still exhibit retained photocatalytic activity after seven runs of 10 h photocatalysis (i.e., 70 h in total; Figure 2a), which proves the high stability of CdS-PD NCs. Considering the high conversion efficiency of CO_2 in the system, we tentatively presume that the main reason for the deactivation should be the lowered concentration of CO_2 rather than the destruction of CdS-PD NCs. Furthermore, when the reaction vessel is enlarged to 150 mL, which has more CO_2 reserves, a higher CO yield of 20.35 mmol g^{-1} h^{-1} and a selectivity of 95.3% are achieved (Table 1, entry 1), confirming the previous presumption.

To identify the key factors for photocatalytic CO_2 reduction, we chose the CdS-PD NCs as the exemplified photocatalyst and performed a series of control experiments. As shown in Table 1 (entry 3−6), when the photoreactions were conducted in the absence of light, CO_2, catalyst, or sacrificial reductant, the reaction systems were completely inactive, demonstrating that all of the above components are indispensable for the photocatalysis. Additionally, when $^{13}CO_2$ (m/z = 45) was used as a reactant, the signal at m/z = 29 corresponding to the ^{13}CO product was detected by the mass spectroscopy measurement (Figure S8), demonstrating that produced CO originates definitely from the photocatalytic reduction of CO_2 over the synthesized CdS NCs.

3.3. Origin of the Superior Photocatalytic Performance of CdS-PD. The above photocatalytic experiment results demonstrate that the CdS NCs modified with the aromatic, conjugated capping ligands exhibit significantly higher activity for photocatalytic reduction of CO_2 to CO than NCs possessing aliphatic capping agents. Especially, CdS-PD NCs possess the highest activity among all of the samples. Previous characterization results on these NCs have shown that the replacement of surface ligands results in insignificant differences in their photophysical properties, such as band gaps and light absorption, as well as the nanoparticle size. Thus, it is unable to correlate the highly distinguished photocatalytic performances with the above properties. Then, based on the structural disparity of the six kinds of capping ligands on the CdS NCs, we initially presume that the electron delocalization in the conjugated ligands enhances the charge mobility and thus the photoreaction rates. This hypothesis can be supported by the results of a series of comparative experiments, which also shed light on the origin of the best photocatalytic performance of CdS-PD. Initially, the photoelectrochemical properties of different ligand-modified CdS NCs are studied by recording the photocurrent density under intermittent light irradiation (Figure 2b). As a result, a much higher photocurrent response for CdS-PD is obtained, demonstrating a significant improvement in the separation of photogenerated carriers. The electrochemical impedance spectroscopy (EIS) was also conducted to investigate the advantages of CdS-PD NCs in the separation of the photogenerated electron and hole (Figure 2c). Generally, the smaller the arc radius in the Nyquist plot, the faster the charge separation and transfer. The results in Figure 2c show that the capping of conjugated ligands on NCs leads to significant improvement in the charge separation and transfer in comparison to those of alkyl ligands, giving the higher charge mobility and thus the better catalytic performances to the corresponding NCs. In addition, it can still be noticed that the CdS-PD NCs display the highest photocurrent response and the charge-transfer ability among all of the samples, inferring that other factors contribute to the high performance besides electron delocalization. Further investigations were made by using transient emission spectroscopy measurements. According to the decay curves (Figure 2d) and the fitting results, the average lifetime of CdS-PD (5.26 ns) is longer than those of other ligand-modified CdS NCs (τ < 4 ns, Table S1). The prolonged lifetime demonstrates the decreased recombination of electron−hole pairs due to the capping of PD ligands, especially in contrast to BZ-capped CdS NCs with only one-atom change in the aromatic ring.

Therefore, apart from the above merits of pyridine ligands, which distribute uniformly on CdS-PD nanocrystals (Figure S9), we speculate that the exposed pyridine sites on the CdS-PD NCs can serve as the active centers to mediate the

https://doi.org/10.1021/acsami.1c03606
ACS Appl. Mater. Interfaces 2021, 13, 26573−26580

reduction of CO_2 on the basis of the following experiments. First, cyclic voltammetry (CV) measurements (Figure S10) were carried out at room temperature under an Ar or CO_2 atmosphere and using a three-electrode cell. The results show that the current of CdS-PD under the CO_2 atmosphere is relatively higher than that obtained under Ar, suggesting the electrocatalytic activity of CdS-PD for CO_2 reduction (Figure S10a). It should be noted that the CV of CdS-PD shows one irreversible reduction wave at −0.55 V vs NHE, attributing to the reduction of protonated pyridinium ligands under the CO_2 atmosphere.[51] As comparable counterparts, the electrochemical behaviors of other non-pyridine ligands CdS-R NCs (R = BZ, NA, OA, MPA, and BF_4) were also investigated by CV measurements. As shown in Figure S10b–f, the reduction peaks of CdS-R from −0.87 to −0.91 V are attributed to the reduction of Cd^{2+} ions on the surface of CdS-R NCs.[56] These results suggest that when compared with CdS NCs capped with inactive ligands, the CdS-PD NCs possess extra electron-transfer mediums after pyridine is protonated. The protonation of pyridine ligands can also be elucidated by the measurement of ζ-potentials. As shown in Figure 3a, without purging of CO_2

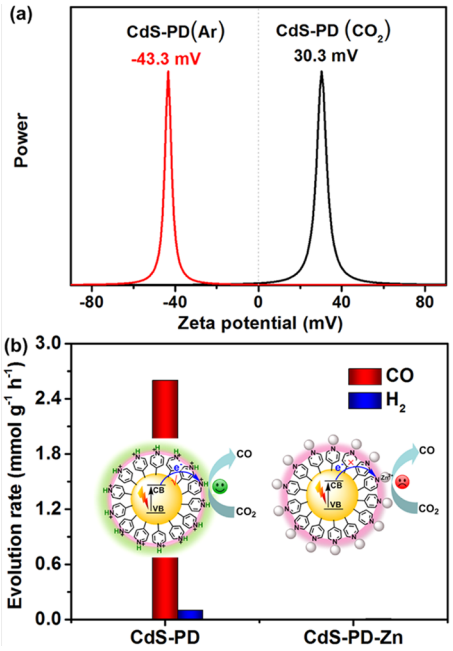

Figure 3. (a) ζ-Potentials of CdS-PD NCs under Ar (red) and CO_2 (black). (b) Comparison of CO yields between CdS-PD and CdS-PD−Zn (with 4.8 mM $ZnCl_2$).

to the reaction solution of CdS-PD NCs, which contains a trace amount of water (403 ppm), the ζ-potential of CdS-PD NCs behaves electronegative (−43.3 mV). In contrast, the potential becomes positive (30.3 mV) when CO_2 is introduced into the solution of CdS-PD NCs. These observations indicate that the injection of acidic CO_2 gas leads to the protonation of pyridine, which can serve as the electron-transfer medium for CO_2 reduction. In addition, we further looked into the effect of the water content on the photocatalytic performance by adjusting the amount of water from 156 to 403 ppm. The results (Figure S11) show a sharp increase of the photocatalytic activity in the range of 156−216 ppm, indicating that a small amount of water plays an important role in the formation of pyridinium catalysts and modulating the photocatalytic activity of CdS NCs. To further illustrate the precatalytic function of pyridine, zinc salt was added as the end-capper to coordinate with pyridine.[57] The results (Figure 3b) show that after adding Zn(II), the catalytic activity of the CdS-PD NC system basically disappeared, suggesting that the pyridine group plays a vital role in the catalytic reduction of CO_2.

3.4. Density Functional Theory (DFT) Calculations for the Catalytic Mechanism. To further verify the catalytic mechanism occurring at the pyridine sites, DFT calculations were operated (Figure 4). Initially, the neutral pyridine moiety

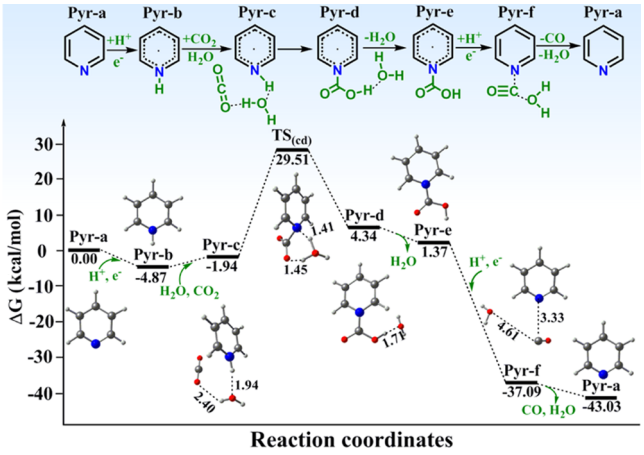

Figure 4. Proposed mechanism and energy diagram for CO_2 reduction catalyzed by pyridine. Optimized structures of the intermediates are shown with gray (carbon), white (hydrogen), red (oxygen), and blue (nitrogen).

(Pyr-a) undergoes a proton-coupled electron-transfer (PCET) process, resulting a protonated radical species (Pyr-b), which can be verified by the electron paramagnetic resonance (EPR) signal in Figure S12 (black line),[58] and the in situ IR spectra (Figure S13) show observed vibrations increase at 1585 and 1660 cm^{-1}, which are assigned to the C═C and C═N vibrations of pyridine, respectively, under light irradiation.[59] Next, Pyr-b can interact with H_2O and CO_2 molecules via hydrogen bonds, corresponding to the Pyr-c species. Through a transition state (TS-cd), the proton can be transferred from the pyridyl nitrogen to the oxygen of CO_2, forming a NCOOH adduct (Pyr-d). The changes of the EPR signal (Figure S12, red line) after CO_2 injection were speculated to the formation of new free radical species, from Pyr-c to Pyr-d. After dehydration (Pyr-e) and the second PCET process (Pyr-f), the C−O bond cleaved and evolved CO. In this process, water plays a key role in the photocatalytic process of CdS-PD nanocrystals. First, the presence of water can protonate pyridine to form pyridinium, which could accept photogenerated electrons from CdS nanocrystals under light irradiation. Second, the H_2O molecule can interact with pyridinium and CO_2 via hydrogen bonds and form a six-membered ring intermediate, leading to a moderate reaction energy barrier, which is consistent with the experimental observations (Figures S11 and S13) and a previous report.[60] Finally, in the proton-coupled electron-transfer mechanism, H_2O can supply the proton to form a NCOOH adduct and facilitate the cleavage of the C−O bond to evolve CO. In the above reaction pathway, the calculated energy barrier is ca. 30 kcal mol^{-1}, which can be easily compensated by light

https://doi.org/10.1021/acsami.1c03606
ACS Appl. Mater. Interfaces 2021, 13, 26573−26580

irradiation, and the whole reaction is exothermic, demonstrating the viability of the pyridine-assisted catalytic mechanism. Thus, it can be concluded that the pyridyl ligand in the CdS NCs can serve as the catalytic center for CO_2 reduction, improving the charge separation and the photocatalytic performance.

4. CONCLUSIONS

In summary, we have successfully prepared a simple CdS-based photocatalyst system for highly efficient CO_2 reduction concomitant with superior selectivity, using dual-functional 4-mercaptopyridine as the surface ligand. The experimental and theoretical results highlight that the protonated pyridinium can delocalize photogenerated carriers and serve as the catalytic active site simultaneously, enhancing the separation and transmission efficiency of photogenerated carriers in contrast to the those of other CdS NCs possessing alkyl-chain and other conjugated capping ligands. Without any cocatalysts, stand-alone CdS-PD NCs achieve an excellent photocatalytic CO_2 reduction activity with a CO yield of 20.35 mmol g^{-1} h^{-1} and a CO selectivity of 95.3%. This work provides a novel and cost-effective strategy for designing high-performance, surface ligand-dependent NCs for artificial photosynthesis.

■ ASSOCIATED CONTENT

Supporting Information

The Supporting Information is available free of charge at https://pubs.acs.org/doi/10.1021/acsami.1c03606.

^{1}H NMR spectra comparison of oleic acid and CdS-PD; TEM images and the Mott−Schottky plots of CdS-R; mass spectrum for the gas generated from the photocatalytic reduction; and EPR spectra of CdS-PD NCs in the reaction solution (PDF)

■ AUTHOR INFORMATION

Corresponding Authors

Wen Zhang − *MOE International Joint Laboratory of Materials Microstructure, Institute for New Energy Materials and Low Carbon Technologies, School of Materials Science and Engineering, Tianjin University of Technology, Tianjin 300384, China;* orcid.org/0000-0001-6105-3286; Email: zhangwen@email.tjut.edu.cn

Min Zhang − *MOE International Joint Laboratory of Materials Microstructure, Institute for New Energy Materials and Low Carbon Technologies, School of Materials Science and Engineering, Tianjin University of Technology, Tianjin 300384, China; Tianjin Key Laboratory of Organic Solar Cells and Photochemical Conversion, School of Chemistry and Chemical Engineering, Tianjin University of Technology, Tianjin 300384, China;* orcid.org/0000-0002-0275-9497; Email: zm2016@email.tjut.edu.cn

Tong-Bu Lu − *MOE International Joint Laboratory of Materials Microstructure, Institute for New Energy Materials and Low Carbon Technologies, School of Materials Science and Engineering, Tianjin University of Technology, Tianjin 300384, China;* orcid.org/0000-0002-6087-4880; Email: lutongbu@tjut.edu.cn

Authors

You-Xiang Feng − *MOE International Joint Laboratory of Materials Microstructure, Institute for New Energy Materials and Low Carbon Technologies, School of Materials Science and Engineering, Tianjin University of Technology, Tianjin 300384, China*

Hong-Juan Wang − *MOE International Joint Laboratory of Materials Microstructure, Institute for New Energy Materials and Low Carbon Technologies, School of Materials Science and Engineering, Tianjin University of Technology, Tianjin 300384, China*

Jia-Wei Wang − *MOE International Joint Laboratory of Materials Microstructure, Institute for New Energy Materials and Low Carbon Technologies, School of Materials Science and Engineering, Tianjin University of Technology, Tianjin 300384, China*

Complete contact information is available at: https://pubs.acs.org/10.1021/acsami.1c03606

Author Contributions

§Y.-X.F. and H.-J.W. contributed equally to this work.

Notes

The authors declare no competing financial interest.

■ ACKNOWLEDGMENTS

This work was financially supported by the National Key R&D Program of China (2017YFA0700104), NSFC (21702146, 21805207, 21790052, 21903060, and 21331007), the Natural Science Foundation of Tianjin City (19JCQNJC05500,17JCJQJC43800), and 111 Project of China (D17003).

■ REFERENCES

(1) Shih, C. F.; Zhang, T.; Li, J.; Bai, C. Powering the Future with Liquid Sunshine. *Joule* **2018**, *2*, 1925−1949.

(2) Xu, S.; Carter, E. A. Theoretical Insights into Heterogeneous (Photo) electrochemical CO_2 Reduction. *Chem. Rev.* **2019**, *119*, 6631−6669.

(3) Li, X.; Yu, J. Z.; Jaroniec, M.; Cen, X. Cocatalysts for Selective Photoreduction of CO_2 into Solar Fuels. *Chem. Rev.* **2019**, *119*, 3962−4179.

(4) Wang, L.; Chen, W.; Zhang, D.; Du, Y.; Amal, R.; Qiao, S.; Wu, J.; Yin, Z. Surface Strategies for Catalytic CO_2 Reduction: from Two-Dimensional Materials to Nanoclusters to Single Atoms. *Chem. Soc. Rev.* **2019**, *48*, 5310−5349.

(5) Fu, X.-Y.; Wei, Z.-Q.; Xu, S.; Lin, X.; Hou, S.; Xiao, F.-X. Maneuvering Intrinsic Instability of Metal Nanoclusters for Boosted Solar-Powered Hydrogen Production. *J. Phys. Chem. Lett.* **2020**, *11*, 9138−9143.

(6) Li, Y.-B.; Li, T.; Dai, X.-C.; Huang, M.-H.; Hou, S.; Fu, X.-Y.; Wei, Z.-Q.; He, Y.; Xiao, G.; Xiao, F.-X. Precise Tuning of Coordination Positions for Transition-Metal Ions via Layer-by-Layer Assembly To Enhance Solar Hydrogen Production. *ACS Appl. Mater. Interfaces* **2020**, *12*, 4373−4384.

(7) Fu, X.-Y.; Li, Y.-B.; Huang, M.-H.; Li, T.; Dai, X.-C.; Hou, S.; Wei, Z.-Q.; Xiao, F.-X. Partially Self-Transformed Transition-Metal Chalcogenide Interim Layer: Motivating Charge Transport Cascade for Solar Hydrogen Evolution. *Inorg. Chem.* **2020**, *59*, 2562−2574.

(8) Li, Y.-B.; Li, T.; Dai, X.-C.; Huang, M.-H.; He, Y.; Xiao, G.; Xiao, F.-X. Cascade Charge Transfer Mediated by in Situ Interface Modulation Toward Solar Hydrogen Production. *J. Mater. Chem. A* **2019**, *7*, 8938−8951.

(9) Xu, S.; Gong, S.; Jiang, H.; Shi, P.; Fan, J.; Xu, Q.; Min, Y. Z-Scheme Heterojunction Through Interface Engineering for Broad Spectrum Photocatalytic Water Splitting. *Appl. Catal., B* **2020**, *267*, No. 118661.

(10) Gong, S.; Jiang, Z.; Shi, P.; Fan, J.; Xu, Q.; Min, Y. Noble-Metal-Free Heterostructure for Efficient Hydrogen Evolution in

Visible Region: Molybdenum Nitride/Ultrathin Graphitic Carbon Nitride. *Appl. Catal., B* **2018**, *238*, 318−327.
(11) Lewis, N. S.; Nocera, D. G. Powering the Planet: Chemical Challenges in Solar Energy Utilization. *Proc. Natl. Acad. Sci. U.S.A.* **2006**, *103*, 15729−15735.
(12) Armaroli, N.; Balzani, V. The Future of Energy Supply: Challenges and Opportunities. *Angew. Chem., Int. Ed.* **2007**, *46*, 52−66.
(13) Wagner, A.; Sahm, C. D.; Reisner, E. Towards Molecular Understanding of Local Chemical Environment Effects in Electro- and Photocatalytic CO_2 Reduction. *Nat. Catal.* **2020**, *3*, 775−786.
(14) Zhang, Y.; Xia, B.; Ran, J.; Davey, K.; Qiao, S.-Z. Atomic-Level Reactive Sites for Semiconductor-Based Photocatalytic CO_2 Reduction. *Adv. Energy Mater.* **2020**, *10*, No. 1903879.
(15) White, J. L.; Baruch, M. F.; Pander, J. E.; Hu, Y.; Fortmeyer, I. C.; Park, J. E.; Zhang, T.; Liao, K.; Gu, J.; Yan, Y.; Shaw, T. W.; Abelev, E.; Bocarsly, A. B. Light-Driven Heterogeneous Reduction of Carbon Dioxide: Photocatalysts and Photoelectrodes. *Chem. Rev.* **2015**, *115*, 12888−12935.
(16) Kou, J.; Lu, C.; Wang, J.; Chen, Y.; Xu, Z.; Varma, R. S. Selectivity Enhancement in Heterogeneous Photocatalytic Transformations. *Chem. Rev.* **2017**, *117*, 1445−1514.
(17) Liu, D.-C.; Zhong, D.-C.; Lu, T.-B. Non-Noble Metal-Based Molecular Complexes for CO_2 Reduction: From the Ligand Design Perspective. *EnergyChem* **2020**, *2*, No. 100034.
(18) Zhang, W.; Mohamed, A. R.; Ong, W. J. Z-Scheme Photocatalytic Systems for Carbon Dioxide Reduction: Where Are We Now? *Angew. Chem., Int. Ed.* **2020**, *59*, 22894−22915.
(19) Sorcar, S.; Yoriya, S.; Lee, H.; Grimes, C. A.; Feng, S. P. A Review of Recent Progress in Gas Phase CO_2 Reduction and Suggestions on Future Advancement. *Mater. Today Chem.* **2020**, *16*, No. 100264.
(20) Wu, L.-Y.; Mu, Y.-F.; Guo, X.-X.; Zhang, W.; Zhang, Z.-M.; Zhang, M.; Lu, T.-B. Encapsulating Perovskite Quantum Dots in Iron-Based Metal−Organic Frameworks (MOFs) for Efficient Photocatalytic CO_2 Reduction. *Angew. Chem., Int. Ed.* **2019**, *58*, 9491−9495.
(21) Zhang, Y.; Yao, D.; Xia, B.; Xu, H.; Tang, Y.; Davey, K.; Ran, J.; Qiao, S.-Z. ReS_2 Nanosheets with In Situ Formed Sulfur Vacancies for Efficient and Highly Selective Photocatalytic CO_2 Reduction. *Small Sci.* **2021**, *1*, No. 2000052.
(22) Li, X.-B.; Tung, C.-H.; Wu, L.-Z. Quantum Dot Assembly for Light-Driven Multielectron Redox Reactions, such as Hydrogen Evolution and CO_2 Reduction. *Angew. Chem., Int. Ed.* **2019**, *58*, 10804−10811.
(23) Guo, Q.; Liang, F.; Li, X.-B.; Gao, Y.-J.; Huang, M.-Y.; Wang, Y.; Xia, S.-G.; Gao, X.-Y.; Gan, Q.-C.; Lin, Z.-S.; Tung, C.-H.; Wu, L.-Z. Efficient and Selective CO_2 Reduction Integrated with Organic Synthesis by Solar Energy. *Chem* **2019**, *5*, 2605−2616.
(24) Jana, A.; Lawrence, K. N.; Teunis, M. B.; Mandal, M.; Kumbhar, A.; Sardar, R. Investigating the Control by Quantum Confinement and Surface Ligand Coating of Photocatalytic Efficiency in Chalcopyrite Copper Indium Diselenide Nanocrystals. *Chem. Mater.* **2016**, *28*, 1107−1120.
(25) Wang, J.; Xia, T.; Wang, L.; Zheng, X.; Qi, Z.; Gao, C.; Zhu, J.; Li, Z.; Xu, H.; Xiong, Y. Enabling Visible-Light-Driven Selective CO_2 Reduction by Doping Quantum Dots: Trapping Electrons and Suppressing H_2 Evolution. *Angew. Chem., Int. Ed.* **2018**, *57*, 16447−16451.
(26) Wu, H.-L.; Li, X.-B.; Tung, C.-H.; Wu, L.-Z. Semiconductor Quantum Dots: An Emerging Candidate for CO_2 Photoreduction. *Adv. Mater.* **2019**, *31*, No. 1900709.
(27) Wang, J.; Feng, Y.-X.; Zhang, M.; Zhang, C.; Li, M.; Li, S.-J.; Zhang, W.; Lu, T.-B. β-Cyclodextrin Decorated CdS Nanocrystals Boosting the Photocatalytic Conversion of Alcohols. *CCS Chem.* **2020**, *2*, 81−88.
(28) Pandya, R.; Steinmetz, V.; Puttisong, Y.; Dufour, M.; Chen, W. M.; Chen, R. Y. S.; Barisien, T.; Sharma, A.; Lakhwani, G.; Mitioglu, A.; Christianen, P. C. M.; Legrand, L.; Bernardot, F.; Testelin, C.; Chin, A. W.; Ithurria, S.; Chamarro, M.; Rao, A. Fine Structure and Spin Dynamics of Linearly Polarized Indirect Excitons in Two-Dimensional CdSe/CdTe Colloidal Heterostructures. *ACS Nano* **2019**, *13*, 10140−10153.
(29) Gao, X.; Han, B.; Yang, X.; Tang, Z. Perspective of Chiral Colloidal Semiconductor Nanocrystals: Opportunity and Challenge. *J. Am. Chem. Soc.* **2019**, *141*, 13700−13707.
(30) Turo, M. J.; Shen, X.; Brandon, N. K.; Castillo, S.; Fall, A. M.; Pantelides, S. T.; Macdonald, J. E. Dual-Mode Crystal-Bound and X-type Passivation of Quantum Dots. *Chem. Commun.* **2016**, *52*, 12214−12217.
(31) Wang, Y.; Pu, C.; Lei, H.; Qin, H.; Peng, X. CdSe@CdS Dot@Platelet Nanocrystals: Controlled Epitaxy, Monoexponential Decay of Two-Dimensional Exciton, and Nonblinking Photoluminescence of Single Nanocrystal. *J. Am. Chem. Soc.* **2019**, *141*, 17617−17628.
(32) Rajendran, V.; Lehnig, M.; Niemeyer, C. M. Photocatalytic Activity of Colloidal CdS Nanoparticles with Different Capping Ligands. *J. Mater. Chem.* **2009**, *19*, 6348−6353.
(33) Wang, P.; Zhang, J.; He, H.; Xu, X.; Jin, Y. The Important Role of Surface Ligand on CdSe/CdS Core/Shell Nanocrystals in Affecting the Efficiency of H_2 Photogeneration from Water. *Nanoscale* **2015**, *7*, 5767−5775.
(34) Turaeva, N. N.; Oksengendler, B. L.; Uralov, I. Synergetics in Multiple Exciton Generation Effect in Quantum Dots. *Appl. Phys. Lett.* **2011**, *98*, No. 243103.
(35) Dong, Y.; Choi, J.; Jeong, H.-K.; Son, D. H. Hot Electrons Generated from Doped Quantum Dots via Up Conversion of Excitons to Hot Charge Carriers for Enhanced Photocatalysis. *J. Am. Chem. Soc.* **2015**, *137*, 5549−5554.
(36) Lian, S.; Weinberg, D. J.; Harris, R. D.; Kodaimati, M. S.; Weiss, E. A. Subpicosecond Photoinduced Hole Transfer from a CdS Quantum Dot to a Molecular Acceptor Bound Through an Exciton-Delocalizing Ligand. *ACS Nano* **2016**, *10*, 6372−6382.
(37) Kuehnel, M. F.; Orchard, K. L.; Dalle, K. E.; Reisner, E. Selective Photocatalytic CO_2 Reduction in Water through Anchoring of a Molecular Ni Catalyst on CdS Nanocrystals. *J. Am. Chem. Soc.* **2017**, *139*, 7217−7223.
(38) Chaudhary, Y. S.; Woolerton, T. W.; Allen, C. S.; Warner, J. H.; Pierce, E.; Ragsdale, S. W.; Armstrong, F. A. Visible Light-Driven CO_2 Reduction by Enzyme Coupled CdS Nanocrystals. *Chem. Commun.* **2012**, *48*, 58−60.
(39) Brown, K. A.; Wilker, M. B.; Boehm, M.; Dukovic, G.; King, P. W. Characterization of Photochemical Processes for H_2 Production by CdS Nanorod−[FeFe] Hydrogenase Complexes. *J. Am. Chem. Soc.* **2012**, *134*, 5627−5636.
(40) Amirav, L.; Alivisatos, A. P. Photocatalytic Hydrogen Production with Tunable Nanorod Heterostructures. *J. Phys. Chem. Lett.* **2010**, *1*, 1051−1054.
(41) Brown, K. A.; Dayal, S.; Ai, X.; Rumbles, G.; King, P. W. Controlled Assembly of Hydrogenase-CdTe Nanocrystal Hybrids for Solar Hydrogen Production. *J. Am. Chem. Soc.* **2010**, *132*, 9672−9680.
(42) William Yu, W.; Peng, X. Formation of High-Quality CdS and Other II−VI Semiconductor Nanocrystals in Noncoordinating Solvents: Tunable Reactivity of Monomers. *Angew. Chem., Int. Ed.* **2007**, *46*, 2559.
(43) Xu, C.; Anusuyadevi, P. R.; Aymonier, C.; Luque, R.; Marre, S. Nanostructured Materials for Photocatalysis. *Chem. Soc. Rev.* **2019**, *48*, 3868−3902.
(44) Cheng, L.; Xiang, Q.; Liao, Y.; Zhang, H. CdS-Based Photocatalysts. *Energy Environ. Sci.* **2018**, *11*, 1362−1391.
(45) Xia, B.; Zhang, Y.; Ran, J.; Jaroniec, M.; Qiao, S.-Z. Single-Atom Photocatalysts for Emerging Reactions. *ACS Cent. Sci.* **2021**, *7*, 39−54.
(46) Tagliazucchi, M.; Tice, D. B.; Sweeney, C. M.; Morris-Cohen, A. J.; Weiss, E. A. Ligand-Controlled Rates of Photoinduced Electron Transfer in Hybrid CdSe Nanocrystal/Poly(viologen) Films. *ACS Nano* **2011**, *5*, 9907−9917.

https://doi.org/10.1021/acsami.1c03606
ACS Appl. Mater. Interfaces 2021, 13, 26573−26580

(47) Hines, D. A.; Kamat, P. V. Quantum Dot Surface Chemistry: Ligand Effects and Electron Transfer Reactions. *J. Phys. Chem. C* **2013**, *117*, 14418−14426.
(48) Li, X.-B.; Gao, Y.-J.; Wang, Y.; Zhan, F.; Zhang, X.-Y.; Kong, Q.-Y.; Zhao, N.-J.; Guo, Q.; Wu, H.-L.; Li, Z.-J.; Tao, Y.; Zhang, J.-P.; Chen, B.; Tung, C.-H.; Wu, L.-Z. Self-Assembled Framework Enhances Electronic Communication of Ultrasmall-Sized Nanoparticles for Exceptional Solar Hydrogen Evolution. *J. Am. Chem. Soc.* **2017**, *139*, 4789−4796.
(49) Lian, S.; Kodaimati, M. S.; Weiss, E. A. Photocatalytically Active Superstructures of Quantum Dots and Iron Porphyrins for Reduction of CO_2 to CO in Water. *ACS Nano* **2018**, *12*, 568−575.
(50) Bi, Q.-Q.; Wang, J.-W.; Lv, J.-X.; Wang, J.; Zhang, W.; Lu, T.-B. Selective Photocatalytic CO_2 Reduction in Water by Electrostatic Assembly of CdS Nanocrystals with a Dinuclear Cobalt Catalyst. *ACS Catal.* **2018**, *8*, 11815−11821.
(51) Barton Cole, B.; Lakkaraju, P. S.; Rampulla, D. M.; Morris, A. J.; Abelev, E.; Bocarsly, A. B. Using a One-Electron Shuttle for the Multielectron Reduction of CO_2 to Methanol: Kinetic, Mechanistic, and Structural Insights. *J. Am. Chem. Soc.* **2010**, *132*, 11539−11551.
(52) Yan, Y.; Zeitler, E. L.; Gu, J.; Hu, Y.; Bocarsly, A. B. Electrochemistry of Aqueous Pyridinium: Exploration of a Key Aspect of Electrocatalytic Reduction of CO_2 to Methanol. *J. Am. Chem. Soc.* **2013**, *135*, 14020−14023.
(53) Boston, D. J.; Xu, C.; D Armstrong, W. F.; MacDonnell, M. Photochemical Reduction of Carbon Dioxide to Methanol and Formate in a Homogeneous System with Pyridinium Catalysts. *J. Am. Chem. Soc.* **2013**, *135*, 16252−16255.
(54) Chang, C. M.; Orchard, K. L.; Martindale, B. C. M.; Reisner, E. Ligand Removal from CdS Quantum Dots for Enhanced Photocatalytic H_2 Generation in pH Neutral Water. *J. Mater. Chem. A* **2016**, *4*, 2856−2862.
(55) Liu, J.; Yang, X.; Wang, K.; Wang, D.; Zhang, P. Chemical Etching with Tetrafluoroborate: A Facile Method for Resizing of CdTe Nanocrystals Under Mild Conditions. *Chem. Commun.* **2009**, *40*, 6080−6082.
(56) Zhao, J.; Holmes, M. A.; Osterloh, F. E. Quantum Confinement Controls Photocatalysis: A Free Energy Analysis for Photocatalytic Proton Reduction at CdSe Nanocrystals. *ACS Nano* **2013**, *7*, 4316−4325.
(57) Topal, T. Synthesis and Characterization of Zinc(II) Complexes with New Pyridine-Based Ligands: Crystal Structure, Hirshfeld Surface Analysis, and Molecular Docking Study of Lung Cancer Cell. *J. Coord. Chem.* **2020**, *73*, 3203−3222.
(58) Thevenon, A.; Rosas-Hernández, A.; Peters, J. C.; Agapie, T. In-Situ Nanostructuring and Stabilization of Polycrystalline Copper by an Organic Salt Additive Promotes Electrocatalytic CO_2 Reduction to Ethylene. *Angew. Chem., Int. Ed.* **2019**, *58*, 16952−16958.
(59) Kamrath, M. Z.; Relph, R. A.; Johnson, M. A. Vibrational Predissociation Spectrum of the Carbamate Radical Anion, C_5H_5N-CO_2^-, Generated by Reaction of Pyridine with $(CO_2)m^-$. *J. Am. Chem. Soc.* **2010**, *132*, 15508−15511.
(60) Wang, L.; Yu, X.; Hu, P.; Broyde, S.; Zhang, Y. A Water-Mediated and Substrate-Assisted Catalytic Mechanism for Sulfolobus solfataricus DNA Polymerase IV. *J. Am. Chem. Soc.* **2007**, *129*, 4731−4737.

https://doi.org/10.1021/acsami.1c03606
ACS Appl. Mater. Interfaces 2021, 13, 26573−26580